Sensors and Materials, Vol. 34, No. 6 (2022) 2199–2212
MYU Tokyo

S & M 2966

Computational Fluid Dynamics (CFD)-based Theoretical Study and *In Vitro* Experimental Evaluation with Sensors for Novel Maglev Nutation Blood Pump

Gang Chen,[1] Li-Gang Yao,[2] Kun-Chieh Wang,[1*] Jia-Xin Ding,[2] and Lei Wu[1]

[1]School of Mechanical and Electric Engineering, Sanming University, Sanming, Fujian Province 365004, China
[2]School of Mechanical Engineering and Automation, Fuzhou University, Fuzhou 350116, China

(Received December 30, 2021; accepted April 5, 2022)

Keywords: maglev, nutation blood pump, numerical simulation, hemolysis test

For a blood pump, high shear stress and bearing wear produced by its high rotational speed are the major factors causing mechanical damage to blood cells inside the pump. To eliminate frictional damage to blood cells, a novel magnetic levitation (maglev) nutation blood pump with low speed and small volume flow is developed in this study. The flow-field characteristics and hemolysis performance of the newly designed blood pump are analyzed and the feasibility of its design is demonstrated. We use computational fluid dynamics and the dynamic grid method to solve the unsteady 3D Navier–Stokes equation in conjunction with the standard k–ε model to simulate and analyze the internal flow field of the blood pump. In an *in vitro* experiment, an *in vitro* circulation loop system including four monitoring sensors is established and fresh sheep blood is used as the circulating medium. The flow pressure is tested by adjusting the speed and load of the pump. To calculate the normalized index of hemolysis (NIH) of sheep blood, its plasma-free hemoglobin and hematocrit levels are detected simultaneously. The prediction results of velocity, pressure, and shear stress distributions in the 3D flow field of the pump demonstrate that our newly designed pump has an antithrombotic property and will not cause serious blood damage. The *in vitro* experiment suggests that a continuous output of more than 5 L/min can be obtained at a 100 mmHg pressure load and that the output flow of the pump is stable at different pressures. The NIH of the nutation pump is 0.0039 ± 0.0006 g/100 L. The research results reveal that our newly designed maglev nutation blood pump has good hemolytic performance and a stable hydraulic property that can meet the requirements for animal experiments.

1. Introduction

Heart transplantation is the most effective means of treating end-stage cardiovascular diseases; however, the application of this surgery is limited by the serious shortage of donor organs and rejection reactions. Artificial hearts can offer an effective alternative to donor

*Corresponding author: e-mail: m18316252102@126.com
https://doi.org/10.18494/SAM3821

ISSN 0914-4935

hearts.[1,2] In this regard, magnetic levitation (maglev) blood pumps, which are characterized by no mechanical contact, no friction, no heating, and low blood damage, have become a research hotspot worldwide.[3,4]

Hemolysis in blood pumps has restricted the development of artificial hearts. Currently, computational fluid dynamics (CFD) is one of the most popular techniques for studying flow-field problems encountered in fluid machinery. Many studies have adopted CFD methods to investigate and predict hemolysis occurring in blood pumps because it could greatly reduce the time and cost of developing new blood pumps.[5] Previously, the internal flow field of a maglev centrifugal blood pump was simulated using CFD and the blood damage caused by the blood pump under various working conditions was investigated.[6] By comparing the results of CFD simulations and *in vitro* hemolysis experiments on a bearing-free centrifugal blood pump, the feasibility of using CFD to study blood damage and improve blood pump designs was demonstrated.[7] Han *et al.*[8] simulated the service states of a centrifugal and axial-flow impeller artificial heart using CFD and predicted the pressure and velocity distributions at the inlet and outlet of the blood pump. Ghadimi *et al.*[9] optimized the structure of a blood pump with the aim of improving its hydraulic performance and reducing blood damage. In practical applications, the frequently used maglev blood pumps, many of which were studied in the aforementioned studies, are mostly centrifugal or axial-flow types. Because of their large size, centrifugal pumps usually have low rotational speeds and are unsuitable for heart implantation. On the other hand, although axial-flow pumps are characterized by small discharge and high efficiency, their high rotor speeds generate large shear stresses that can easily damage blood cells.[10]

To overcome the aforementioned defects of traditional centrifugal and axial-flow maglev blood pumps in heart implantation, the concept of the nutation drive has been introduced. This is a drive mode based on the principles of the motion governing planets and celestial bodies.[11] The principles of nutation motion have been widely applied in many engineering fields, such as gear drives, manipulators, motors, and space probes.[12] He *et al.*[13] proposed a nutation blood pump with mechanical bearings, which follows the principles of the nutation drive. This blood pump rotor was driven by a motor shaft via an inclined sleeve so as to induce nutation motion. The angle between the rotation axis of the motor and the bore axis of the inclined sleeve is referred to as the nutation angle. However, in the above studies, the rotor is in direct contact with the supporting spherical joints inside the pump chamber; thus, substantial mechanical wear is inevitable and blood cells are easily damaged and contaminated.

To overcome these defects of a nutation blood pump, here we propose a novel design for a maglev nutation blood pump with permanent magnets, which may solve the problems of blood wear and damage. We also analyze the structure and operating principles of the contactless magnetic drive as well as the magnetically levitated bearings for the newly designed pump. By simulating the internal flow field of the newly designed blood pump using CFD, we theoretically obtain the distributions of the velocity, pressure, shear stress, and other key parameters of the blood flow in the pump, and therefore demonstrate its superiority. In addition, an *in vitro* hemolysis experiment is performed using the proposed new blood pump for verification.

2. Newly Designed Blood Pump: Operating Principles and Structures

Nutation blood pumps feature the advantages of low rotational speed, similarly to centrifugal blood pumps, and small volume flow rate, similarly to axial-flow blood pumps. Thus, they are more suitable than other blood pumps for generating a normal human blood flow with a rate of about 5 L/min.[14] However, nutation blood pumps with bearings induce mechanical contact wear between the blood and the components inside the pump, which may cause low blood compatibility.

Figure 1 shows the inner structure of the proposed maglev nutation blood pump. This unique design comprises a contactless magnetic drive and magnetically levitated bearings with permanent magnets. First, several axially magnetized fan-shaped permanent magnets are installed at regular intervals around the edge of the nutation disk. Second, two motor-driven permanent magnets (Magnet 1 and Magnet 2, see Fig. 1) with opposite magnetization directions are placed on the top of the pump. The upper permanent magnets at the edge of the nutation disk are attracted to Magnet 1 at one end and repulsed by Magnet 2 at the other end. In this way, the nutation disk can always maintain a tilted state. The tilting angle is called the nutation angle. The directional rotation of driving induced by Magnets 1 and 2 will cause the permanent magnets to move to different positions around the nutation disk, generating upward motion on one side and downward motion on the other side. This upward and downward oscillatory motion of the disk induced contactlessly by the magnets is referred to as "nutation motion". There is no gap between the nutation disk and the upper and lower covers. As the blood flows into the inlet of the pump, the blood pressure gradually increases with the increasing area at the inlet. While the blood flows into the outlet of the pump, the blood pressure gradually decreases with the decreasing area at the outlet. The resultant pressure gradient between the inlet and outlet drives the blood flow through the pump tunnel continuously.

Permanent magnetic rings are installed inside the rotor and pump cover to control the levitation state of the blood pump rotor. Figure 2 shows a photograph of the proposed maglev

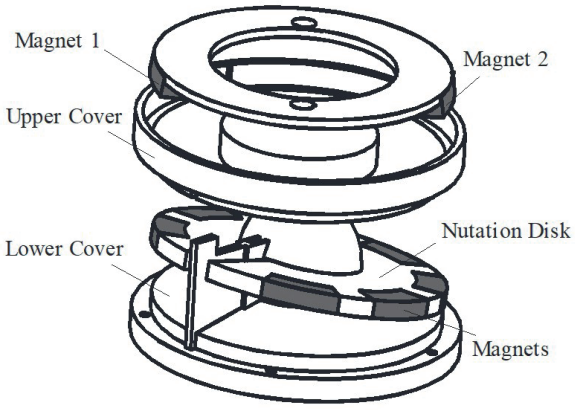

Fig. 1. Inner structure of the newly designed maglev nutation blood pump.

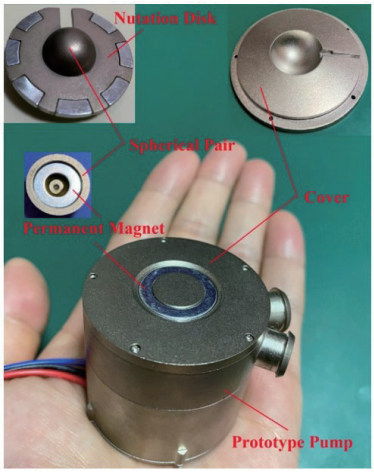

Fig. 2. (Color online) Newly designed maglev nutation blood pump and its components.

nutation blood pump. The nutation disk is supported at the center of the pump by upper and lower spherical joints, which both have permanent magnetic rings inside them. Permanent magnetic rings are also installed inside the pump cover. The permanent magnetic rings inside the spherical joints and those inside the pump cover are mutually repulsive. The magnetic action of the permanent magnetic rings installed inside the upper and lower covers and spherical joints provides contactless support of the blood pump rotor, thereby reducing blood wear and blood contamination.

3. Numerical Simulation of Blood Flow in Newly Designed Pump

3.1 Computational model, meshing, and boundary conditions

First, we design the configuration of the flow channel for our proposed pump using computer-aided design (CAD) software. The computational region of the flow channel is composed of the rotor body, inlet and outlet regions, lower and upper cover regions, and inner surface region of the pump shell. The inner surfaces of the spherical joints in the rotor and the pump shell are spherical, whereas the surfaces of the upper and lower covers of the pump are conical. The computational region is divided into two parts according to the complexity of the geometry. Second, a Boolean subtraction operation is applied to the 3D geometric model, and the configuration model of the flow channel is then exported to a CFD software package for flow-field meshing as pre-processing.

The motion of the rotor causes severe changes to the flow conditions. Therefore, we specifically adopt a dynamic meshing scheme to simulate the ever-changing flow conditions in the blood pump. Note that the complex wedge-shaped region between the nutation disk and the upper and lower covers usually causes a poor meshing condition in the computation. In other words, when the moving part is defined in a dynamic mesh system, the constructed dynamic mesh may easily be distorted in the reconstruction process, resulting in unreasonable parameter values such as negative volumes. Thus, to avoid the straight-line contact, we modify the geometry of the mesh for the flow field during the CFD meshing process. An opening of 0.1 mm width is set between the upper surface of the nutation disk and the upper cover of the pump and also between the lower surface of the nutation disk and the lower cover of the pump. Since the configuration of the nutation blood pump is geometrically complex, we adopt a suitable unstructured tetrahedral mesh. Figure 3 shows the meshing result of the blood flow field, which has a total of 620157 mesh elements without any mesh distortion or negative values.

3.2 Governing equations

Assuming that the working medium of blood is an incompressible viscous non-Newtonian fluid, the governing equation of mass conservation can be expressed as

$$\frac{\partial \rho}{\partial t} + \frac{\partial (\rho u)}{\partial x} + \frac{\partial (\rho v)}{\partial y} + \frac{\partial (\rho w)}{\partial z} = 0, \tag{1}$$

Fig. 3. Mesh model of the maglev nutation blood pump.

where ρ is the density of blood, t is the time, and u, v, and w are the components of the fluid velocity in the x, y, and z directions, respectively.

The governing equation for the conservation of momentum (Navier–Stokes equation) can be expressed as

$$\begin{cases} F_x - \frac{1}{\rho}\frac{\partial p}{\partial x} + v\left(\frac{\partial^2 u_x}{\partial x^2} + \frac{\partial^2 u_x}{\partial y^2} + \frac{\partial^2 u_x}{\partial z^2}\right) = \frac{du_x}{dt}, \\ F_y - \frac{1}{\rho}\frac{\partial p}{\partial y} + v\left(\frac{\partial^2 u_y}{\partial x^2} + \frac{\partial^2 u_y}{\partial y^2} + \frac{\partial^2 u_y}{\partial z^2}\right) = \frac{du_y}{dt}, \\ F_z - \frac{1}{\rho}\frac{\partial p}{\partial z} + v\left(\frac{\partial^2 u_z}{\partial x^2} + \frac{\partial^2 u_z}{\partial y^2} + \frac{\partial^2 u_z}{\partial z^2}\right) = \frac{du_z}{dt}, \end{cases} \tag{2}$$

where F_x, F_y, and F_z are the components of the unit mass force in the x, y, and z directions and u_x, u_y, and u_z are the components of velocity along the x, y, and z axes, respectively.

The law of conservation of energy is derived from the first law of thermodynamics. We suppose that the temperature changes or heat exchange in the blood pump can be neglected. Since the human body temperature is approximately constant, the internal energy of the fluid in the blood pump can also be assumed constant. On the basis of these concepts, the governing equation for the conservation of energy can be written as

$$\frac{1}{2}\rho(u^2 + v^2 + w^2) + \rho g h + p = const, \tag{3}$$

where the first, second, and third terms on the left side are the kinetic energy, gravitational potential energy, and pressure potential energy of the fluid element, respectively.

3.3 Numerical method

The above governing equations for the transient flow field of the blood pump are numerically solved using CFD software. The standard k–ε model is adopted as the turbulence model. The problem of the near-wall flow in the blood pump is solved using the standard wall-function

method. The mesh of the flow field is updated dynamically by smoothing and remeshing techniques. The inner and outer spherical surfaces of the blood pump in the flow channel are set as the deformation planes and the nutation disk is viewed as a rigid body. The computational time step and the convergence residual are set as 10^{-4} and 10^{-6} s, respectively.

4. Results Obtained by CFD Method and Discussion

4.1 Hydraulic performance

A stable output flow rate is one of the most important requirements for a blood pump. Normal adults usually have a cardiac output of about 5 L/min and an arterial blood pressure ranging from 80 to 120 mmHg. Figures 4 and 5 show the output flow rates of the blood pump calculated at different rotational speeds and pressure differences between the inlet and outlet, respectively. To reasonably simulate a human adult's heart, the designed rotor of the blood pump must be

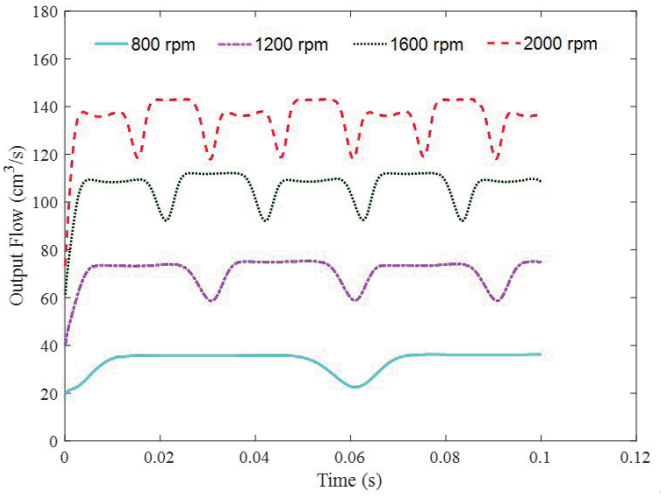

Fig. 4. (Color online) Output flow rate at different rotational speeds.

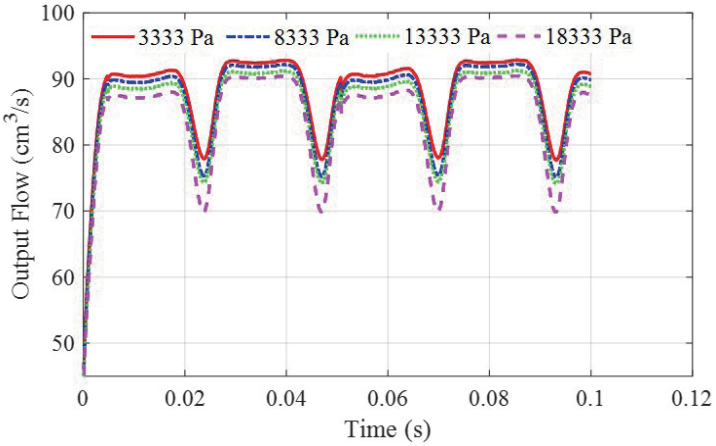

Fig. 5. (Color online) Output flow rate at different pressure differences between the inlet and outlet.

capable of rotating at 1300 rev/min at the output flow rate of 5 L/min and at the pressure difference between the inlet and outlet of 100 mmHg, which we adopt as the standard working conditions for analyzing the internal flow field of the blood pump.

On the whole, the change in the output flow rate versus time is approximately a horizontal line, indicating that the output flow rate of the blood pump is reasonably stable. Upon reaching integral multiples of the half cycle, the flow rate curve becomes slightly concave for an extremely short period (e.g., a duration of 0.0072 s for a flow rate drop of 18.6 cm^3/s at a rotational speed of 1600 rev/min). This phenomenon occurs because of a specific feature of the design: an opening set on the fixed connection between the nutation disk and the rotor. The contact region between the nutation disk and the pump cover disappears immediately as the disk moves to the opening. This effect leads to a transient disconnection between the inlet and the outlet, resulting in a periodic variation of the output flow rate, which suddenly drops at certain times and then rises immediately. Normal adults usually have an average heart rate of about 75 beats/min, and the whole ejection process takes about 0.8 s to complete. The working cycle of the maglev nutation blood pump at a rotational speed of 1300 rev/min and an output flow rate of 5 L/min is 0.046 s. This means that for every half cycle, the flow rate decreases for an extremely short period of time but this does not appear to affect the blood supply. Thus, it is concluded from the variation of the output flow rate versus time that the outflow of the nutation blood pump is stable.

4.2 Distributions of velocity and pressure

Figure 6(a) shows the calculated velocity vector distribution in the internal flow field of the maglev nutation blood pump at the start-up stage under standard working conditions. The blood

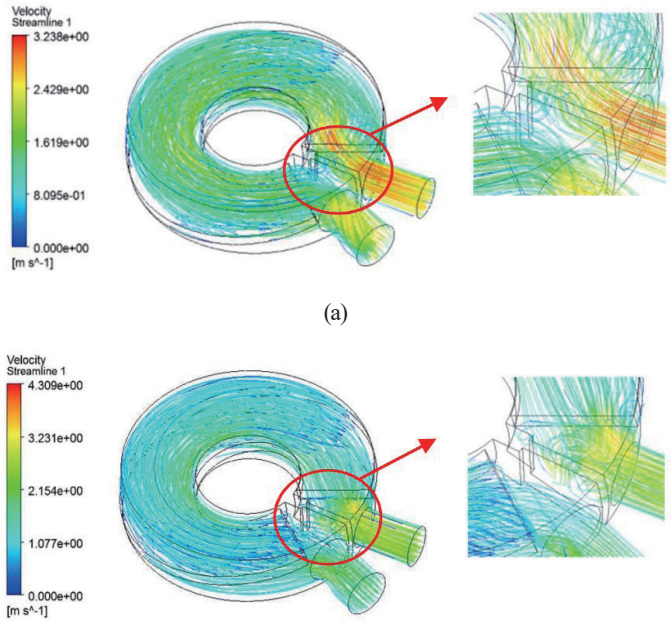

Fig. 6. (Color online) Velocity streamline of flow field in the maglev nutation blood pump. (a) $t = 0.004$ s (just after pump start-up). (b) $t = T$ (during stable period of time).

flow has a consistent trend of a low overall flow rate and small velocity gradient, and there is no dead zone in the entire flow field. A slight local backflow occurs near the outlet in the vicinity of the opening of the nutation disk, which is caused by the temporarily unstable flow just after the start-up time of the pump. Figure 6(b) shows the streamline distribution of the flow field at the periodic stable operation stage. The flow rate in the flow channel of the blood pump increases with increasing flow velocity. Moreover, high-velocity flows occur near the outlet with a maximum flow rate of 4.3 m/s. This may be attributed to the effect of the small cross-sectional area and high pressure at the outlet. Local backflow persists near the outlet, especially in the vicinity of the opening of the nutation disk where the nutation disk does not come in contact with the upper and lower covers. Moreover, when fluid flows from the upper part of the nutation disk through the opening to the outlet, the effect of the height difference will induce a small backflow in the opening region.

By solving Eqs. (1)–(3) via the CFD method, we obtain the pressure distribution for the flow field, and the resultant pressure nephograms are shown in Fig. 7. The contact region between the nutation disk and the pump cover divides the internal space of the blood pump into low- and high-pressure zones. The pressure in the high-pressure zone is slightly higher than the preset outlet pressure of 114658 Pa, and the pressure in the low-pressure zone is slightly lower than the preset inlet pressure of 101325 Pa. The low-pressure zone is connected to the inlet, inducing the "water-absorbing" effect, whereas the high-pressure zone is connected to the outlet, inducing the "water-pressurizing" effect. In the high-pressure zone, the pressure is particularly high close to the outer side of the flow channel and particularly low close to the inner side because of the circulating motion of the fluid caused by centrifugal forces. Overall, the pressure is distributed uniformly in both the high-pressure zone and the low-pressure zone.

4.3 Distribution of shear stress

Figure 8 shows the obtained wall shear stress nephograms of the nutation disk surfaces under standard working conditions. It is found that the wall shear stress is high around the contact region with a maximum value of 620 Pa and small elsewhere. According to an experimental study by Chen *et al.*,[15] blood hemolysis has a strong relationship with the shear stress and

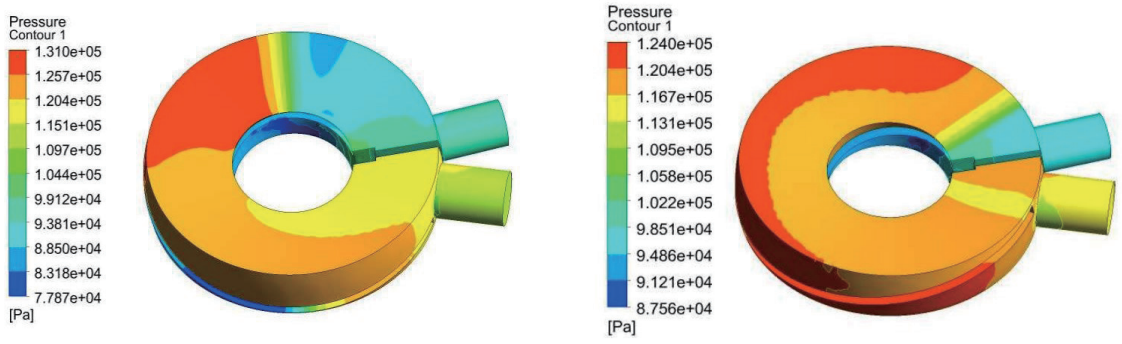

(a) (b)

Fig. 7. (Color online) Pressure nephograms of flow field in the maglev nutation blood pump. (a) $t = 0.25\ T$. (b) $t = 1\ T$.

duration of exposure of red blood cells (RBCs), and when the shear stress is lower than 150 Pa, RBCs will not be damaged even if their exposure duration is infinitely long. Figure 9 shows the calculated shear stress distribution. It can be seen that about 90% of the shear stress values are smaller than 150 Pa. Large shear stresses (greater than 150 Pa) mainly occur near the high-velocity region, where the duration of RBC exposure is extremely short. Therefore, RBCs in the blood pump are not susceptible to wearing-induced damage and our newly designed blood pump is theoretically proved to have good hemolytic performance.

To further clarify the status of blood damage in the blood pump, four shear stress monitoring points are set at the inlet, outlet, inner wall, and outer wall. Figure 10 illustrates these four monitoring positions, denoted as Monitoring Point 1 ($X = -0.0184$ mm, $Y = 0$, $Z = 0.0043$ mm), Monitoring Point 2 ($X = -0.0076$ mm, $Y = 0$, $Z = 0.0025$ mm), Monitoring Point 3 ($X = -0.0180$ mm, $Y = 0.0042$ mm, $Z = 0.0043$ mm), and Monitoring Point 4 ($X = 0.0181$ mm, $Y = -0.0037$ mm, $Z = 0.0043$ mm).

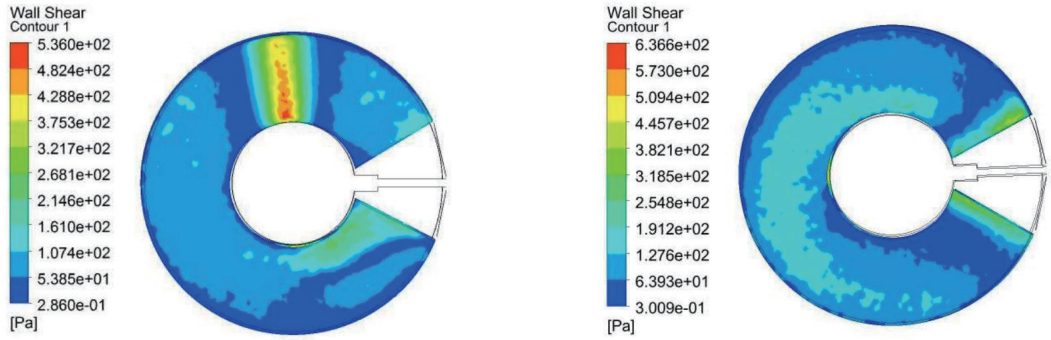

(a) (b)

Fig. 8. (Color online) Wall shear stress nephograms of the nutation disk. (a) $t = 0.25$ *T*. (b) $t = 1$ *T*.

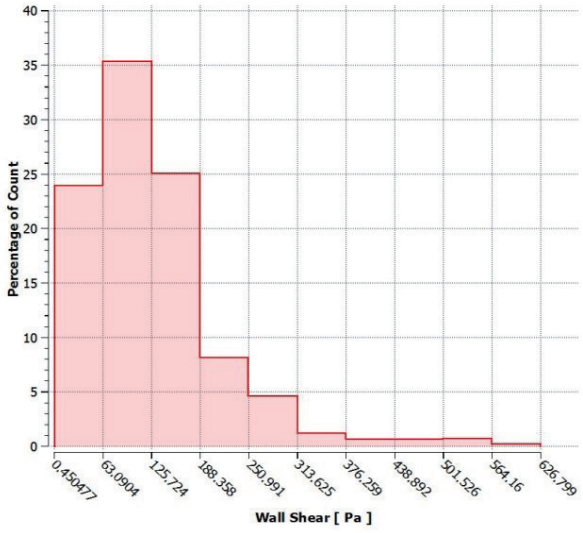

Fig. 9. (Color online) Histogram of shear stress distribution.

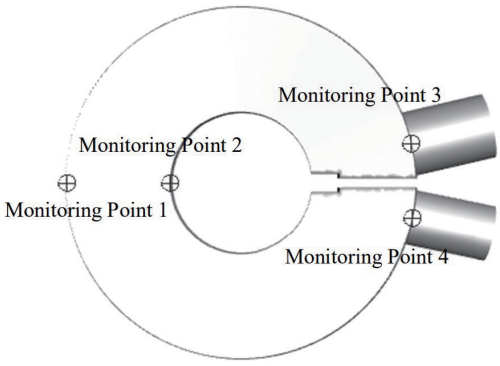

Fig. 10. Monitoring points for the flow field in the blood pump.

Figure 11 shows the changes in the wall shear stress at the four monitoring points in one operation cycle under standard working conditions. The wall shear stresses at Monitoring Points 1 and 2 vary within the range of 600–700 Pa in the initial 0.0015 s. Between 0.0015 and 0.003 s, just after the time of pump start-up, the wall shear stresses at Monitoring Points 1 and 2 first decrease rapidly to 103 Pa, then remain below 100 Pa. The shear stresses at Monitoring Points 3 and 4 are stable and always below 100 Pa. The wall shear stresses at Monitoring Points 1 and 2 are large in the initial 0.0015 s because these monitoring points are located exactly on the contact region where a high velocity gradient occurs at the moment of pump start-up. After 0.0015 s, the contact region moves away from the monitoring positions, and the wall shear stresses at these positions drop abruptly. From these results, it is found that the wall stresses in the blood pump are extremely low and too low to damage RBCs during most of the pump operation time. The large wall shear stresses at the contact region are only for a very short time and are unlikely to damage RBCs.

5. *In Vitro* Experiment

5.1 Experiment methods

An *in vitro* hemolysis experiment is conducted using fresh goat blood as the working fluid of the designed pump. The experiment is repeated four times. For every experiment, 500 ml of blood is collected in a blood bag and 250 U of heparin is added for anti-coagulation treatment. The circulating pipe system is composed of a blood storage tank (Dongguan Kewei Medical Instrument Co.), a water bath, a heparin-coated pipe line, a pressure-regulating valve, a manometer (GM520, Jumaoyuan Science and Technology Co.), a flowmeter (Model K24, Bangsheng Machinery Co.), an IR thermometer (Model DT8300B, Cheerman Co.), and the proposed blood pump. Figure 12 shows a schematic diagram of the *in vitro* circulating experimental facility used to test the hydraulic and hemolytic performance of our designed blood pump. Air is vented through the exhaust port of the blood storage tank to reduce RBC

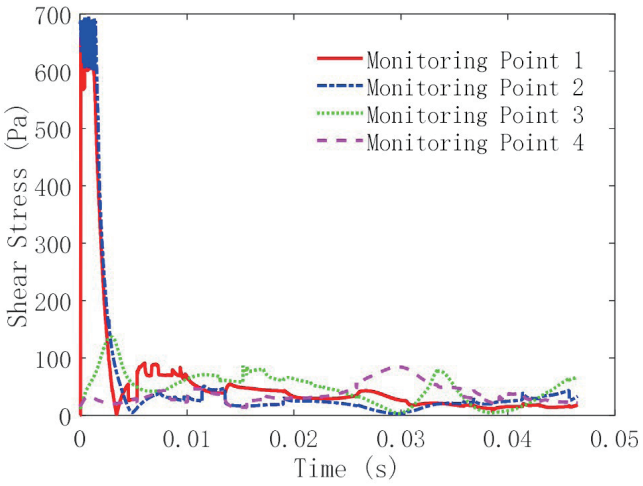

Fig. 11. (Color online) Shear stress of the four monitoring points in one period.

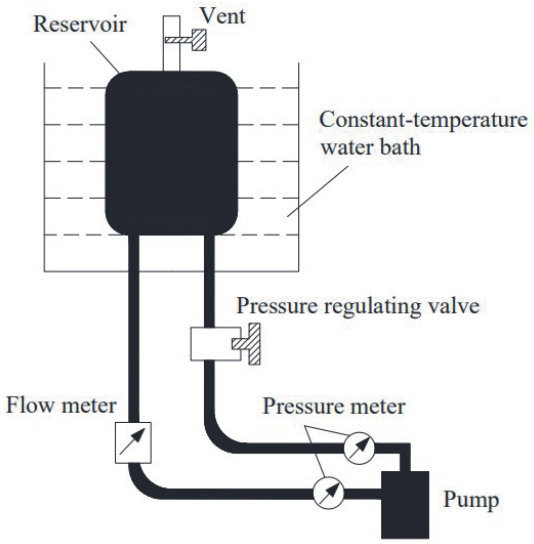

Fig. 12. *In vitro* circulation loop system.

damage caused by air bubbles. After turning on the blood pump, its rotational speed is adjusted to 1450 rpm. The actual output flow rate at this rotational speed is about 5 L/min. The height of the blood storage tank is regulated so as to generate a preload of 15 mmHg. Meanwhile, the pressure-regulating value is set to generate a normal load of 100 mmHg. Blood samples (5 mL each time) are collected from the blood storage tank before pump start-up and at 60, 120, 180, and 240 min after start-up. Then, we measure the free hemoglobin (denoted as *FHb*) and hematocrit (denoted as *Hct*) levels of the collected blood samples, and use them to calculate the hemolysis value. Two pressure sensors are set near the pump inlet and outlet and the flowmeter is set at the outlet. With these fluid sensors, the hydraulic performance of the blood pump is determined by measuring the pressure difference between the inlet and outlet, and the output flow rate at five different rotational speeds.

5.2 Experimental results

The blood pump operates normally during all four experiments. *FHb* and *Hct* are measured at each preset time and then used to calculate the hemolysis value of the pump. The test results are shown in Table 1. The normalized index of hemolysis (NIH_{exp}, unit: g/100 L) is calculated using the following formula:[16]

$$NIH_{exp} = \Delta FHb \times (100 - Hct) \times \frac{Vol}{Q \times \Delta t}, \tag{4}$$

where ΔFHb (unit: g/L) is the increment of blood-free hemoglobin during the test interval, Vol is the circulating volume (unit: m^3), Q is the volume flow rate (unit: m^3/min), and Δt is the sampling time (min).

Table 1
Results of *in vitro* hemolysis test (n = 16).

Group	*Hct* (%)	NIH_{exp} (g/100 L)			
		60 min	120 min	180 min	240 min
1	34.2	0.0035	0.0039	0.0044	0.0043
2	33.6	0.0033	0.0032	0.0041	0.0046
3	33.4	0.0031	0.0034	0.0036	0.0042
4	33	0.0034	0.0038	0.0046	0.0051

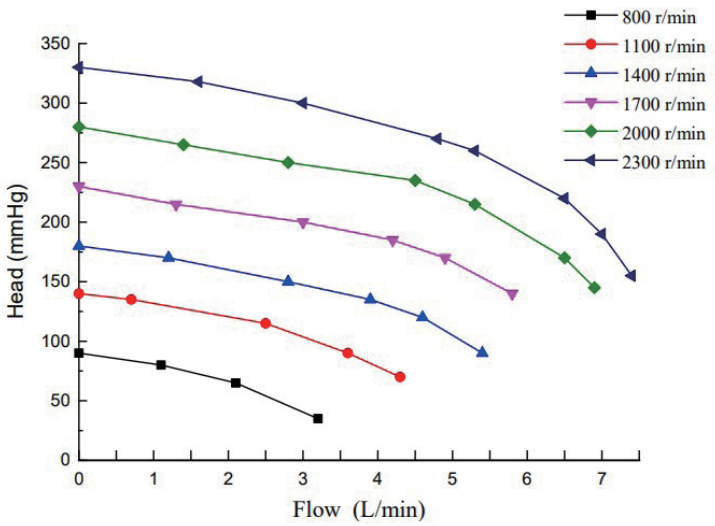

Fig. 13. (Color online) Hydraulic performance of the blood pump.

All experimental results are statistically analyzed. The mean and standard deviation of the experimental data are calculated as 0.0039 and 0.0006 g/100 L, respectively. The NIH is calculated as 0.0039 ± 0.0006 g/100 L. Hemolytic performance is an important index for assessing blood pump performance. The results of the *in vitro* hemolysis experiment indicate that the NIH of our newly designed maglev nutation blood pump is slightly lower than the hemolysis index of other types of blood pump[17] but more accurate than those of centrifugal and axial-flow blood pumps.[18,19] Figure 13 shows the experimental results for the hydraulic performance of our newly designed blood pump. At a rotational speed of 1450 rpm and a pressure of 100 mmHg, the output flow rate is measured with a flowmeter to be 5 L/min, which can meet the requirements of left ventricular assist devices used in clinics.[20]

6. Conclusion

Compared with the current mainstream maglev blood pumps, our proposed novel pump has an obvious advantage of providing a suitable blood flow rate (5 L/min) at a low rotational speed (1300 rpm). For example, to provide a stable blood flow rate of about 5 L/min, the CentriMag and Arrow CorAide blood pumps must operate at over 4000 and 2750 rpm, respectively. The low operational speed of the proposed nutation blood pump may significantly reduce the shear stress

of blood, thus reducing damage to blood cells. In this study, the CFD method is used in conjunction with a dynamic meshing technique to numerically simulate the internal flow field of the proposed maglev nutation blood pump and simultaneously predict the hemolysis value of blood in the pump. Some *in vitro* experiments with pressure sensors and flowmeters are also performed to verify the calculated results. The main findings of this study can be summarized as follows:

(1) The size of the opening of the nutation disk of the maglev nutation blood pump affects the flow stability as well as the output flow rate of the pump. The flow rate suddenly decreases when the contact region moves to the opening position. The higher the rotational speed, the lower the flow rate.

(2) Overall, the flow field of our newly designed blood pump has a low fluid velocity and velocity gradient, and there is no backflow. Large shear stresses only temporarily occur around the contact region between the nutation disk and the upper cover and between the nutation disk and the lower cover. The shear stresses are low in the entire flow region except around the contact region of the blood pump.

(3) The experimental results indicate that the NIH of the maglev nutation blood pump is small and that the hydraulic performance of the blood pump can meet the flow rate and pressure requirements. It is concluded that our newly designed blood pump is suitable for use as a left ventricular assist device in clinics. In addition, this approach allows us to effectively assess the positions of high shear stress, which helps optimize the blood pump structures and promote further experimental research. Moreover, our findings provide vital guidance toward the design of *in vivo* experiments and blood pump structures better suited to the flow characteristics of human blood.

Acknowledgments

This work was supported in part by the Development Projects of Central Government Guided Local Science and Technology under Grant no. 2021L3046, in part by the Technology Plan Guiding Project of Sanming under Grant no. 2020-G-58, and in part by Sanming University of Fujian Province, China, under Grant no. 19YG05.

References

1 K. Thangappan, A. Ashfaq, C. Villa, and D. L. S. Morales: Ann. Cardiothorac Sur. **9** (2020) 89. https://doi.org/10.21037/acs.2020.02.08
2 F. A Arabía: Ann. Cardiothorac Sur. **9** (2020) 68. https://doi.org/10.21037/acs.2020.02.05
3 K. Huynh: Nat. Rev. Cardiol. **14** (2017) 1. https://doi.org/10.1038/nrcardio.2016.199
4 D. Mozaffarian, E. J. Benjamin, A. S. Go., D. K. Arnett, and M. J. Blaha: Circulation **133** (2016) 447. https://doi.org/10.1161/CIR.0000000000000409
5 H. M. P. Rosa and B. S. Emerick: Revista Brasileira de Engenharia Agrícola e Ambiental **24** (2020) 3. https://doi.org/10.1590/1807-1929/agriambi.v24n1p3-7
6 P. Aigner, T. Schlogthofer, D. Fechtig, and M. Schima: Int. J. Artif. Organs **36** (2013) 542. https://doi.org/10.5301/ijao.5000244
7 P. Pascal, S. Marcel, and K. Johann W: IEEE Trans. Bio-Med. Eng. **68** (2020) 1370. https://doi.org/10.1109/TBME.2020.3030316

8 Q. Han, X. D. Ruan, W. Y. Chen, and X. Fu: Chin. J. Mech. Eng-En. **5** (2013) 967. https://doi.org/10.3901/CJME.2013.05.967
9 B. Ghadimi, A. Nejat, S. A. Nourbakhsh, and N. Naderi: J. Artif. Organs **22** (2019) 29. https://doi.org/10.1007/s10047-018-1072-z
10 P. Puentener, M. Schuck, and W. Kolar J: IEEE T. Bio-Med. Eng. **68** (2021) 1370. https://doi.org/10.1109/TBME.2020.3030316
11 Z. Lin, L. G. Yao, J. Zhang, and T. K. Su: J. Braz. Soc. Mech. Sci. **42** (2020) 10. https://doi.org/10.1007/s40430-019-2085-0
12 Z. Lin, L. G. Yao, and Z. Y. Xie: Mech. Sci. **11** (2020) 115. https://doi.org/10.5194/ms-11-115-2020
13 J. Y. He, L. G. Yao, H. W. Shen, and R. Y. Zheng: Procedia CIRP **36** (2015) 273. https://doi.org/10.1016/j.procir.2015.08.034
14 G. Chen, L. G. Yao, R. Y. Zheng, L. Zhang, and J. X. Ding: IEEE Access **7** (2019) 169327. https://doi.org/10.1109/ACCESS.2019.2955027
15 Z. S. Chen, S. K Jena, G. A Giridharan, and M. A Sobieski: Med. Biol. Eng. Comput. **57** (2019) 807. https://doi.org/10.1007/s11517-018-1922-0
16 K. Ryo, S. Daisuke, N. Masahiro, M. Osamu, and Y. Takashi: J. Artif. Organs **1** (2021) 157. https://doi.org/10.1007/s10047-020-01240-6
17 L. F. Zhu, Y. Wu, and Y. Luo: Int. J. CARS. **11** (2016) 173. https://doi.org/10.3233/JAE-162159
18 D. L. Wang, J. P. Tan, and Z. Q. Yu: J Central South University (Science and Technology) **49** (2018) 1929. https://doi.org/10.11817/j.issn.1672-7207.2018.08.013
19 L. V. Belyaev, A. B. Ivanchenko, A. V. Zhdanov, and V. V. Morozov: Biomed. Eng. **51** (2017) 77. https://doi.org/10.1007/s10527-017-9688-5
20 L. F. Zhu, Y. Wu, and Y. Luo: Int. J Appl. Electron. **52** (2016) 525. https://doi.org/10.3233/JAE-162159